Journal of Marine Systems 241 (2024) 103893

Contents lists available at ScienceDirect

Journal of Marine Systems

journal homepage: www.elsevier.com/locate/jmarsys

Sources and distribution of dissolved organic matter and inorganic nitrogen in waters of the southern Patagonian shelf and northern Drake Passage (51–56°S, 64–69°W)

John E. Garzón-Cardona [a,b,*], Ana M. Martínez [b,c], Boris P. Koch [d,e], Bernd Krock [d], Elbio D. Palma [a,f], Xianyu Kong [d], Rubén J. Lara [a]

[a] Instituto Argentino de Oceanografía (IADO, CONICET-UNS), Bahía Blanca, Argentina
[b] Departamento de Química, Universidad Nacional del Sur (UNS), Bahía Blanca, Argentina
[c] Instituto de Química del Sur, INQUISUR-CONICET-UNS, Av. Alem 1253, B8000FWB Bahía Blanca, Argentina
[d] Alfred-Wegener-Institut Helmholtz Zentrum für Polar - und Meeresforschung, Ökologische Chemie, Am Handelshafen 12, 27570 Bremerhaven, Germany
[e] Hochschule Bremerhaven, University of Applied Sciences, An der Karlstadt 8, D-27568 Bremerhaven, Germany
[f] Departamento de Física, Universidad Nacional del Sur (UNS), Bahía Blanca, Argentina

ARTICLE INFO

Keywords:
Dissolved organic carbon
Inorganic nitrogen
Southern Patagonian shelf

ABSTRACT

Dissolved organic matter (DOM) plays a crucial role in the biogeochemistry of coastal ecosystems, particularly nutrient cycling and distribution. Little is known about these processes in the highly productive Southern Patagonian shelf. This study was conducted to better understand the sources, composition, and behavior of DOM and inorganic nutrients in the sector between 51 and 56°S and 64–69°W with particular emphasis on inorganic nitrogen and DOM fractions. Surface water samples taken during late austral summer from the Beagle Channel (BCW), Subantarctic (SAW), Subantarctic Shelf (SASW), Grande Bay (GBW) and Tierra del Fuego Waters (TFW) and were analyzed for properties of fluorescent DOM (FDOM), dissolved organic carbon (DOC) and inorganic nutrients. Data were related to hydrographic and plankton conditions. Highest values of ammonium, DOC, humic-like FDOM ($FDOM_C$ and $FDOM_M$ peaks) and humification index (HIX) were found in BCW, and the lowest in SAW, suggesting that terrigenous input is a main source of ammonium and refractory carbon in this region, which is supported by a highly significant inverse correlation of these parameters with salinity. In contrast, nitrate, phosphate, silicate and the fluorescence index (FI) were positively correlated with salinity, pointing to the contribution of autochthonous FDOM from the saltier and nutrient-rich Antarctic Circumpolar Current to the Southern Patagonian shelf. In TFW and GBW, high nitrite concentrations, accompanied by elevated values of BIX (biological activity index of DOM), circulation patterns and high particle residence times computed from model results suggest the occurrence of regeneration processes that deserve further investigation of the poorly known dynamics of the nitrogen-rich water in this region.

1. Introduction

Scarce information is available about the origin, distribution and dynamics of dissolved organic matter (DOM) and inorganic nitrogen (DIN) in the highly productive waters of the Southern Patagonian shelf (Fig. 1) (Lara et al., 2010; Paparazzo and Esteves, 2018). DOM fractions play a significant role in the biogeochemical processes of the Pacific-Atlantic connection (Barrera et al., 2017), facilitating the challenging tracking of carbon and nutrient sources in this highly complex sector. In previous work (Garzón-Cardona et al., 2016; Giesecke et al., 2021; Iachetti et al., 2021), we identified patterns of ammonium and nitrate distribution clearly related to sources in the Beagle Channel and related fjord systems and to the Antarctic Circumpolar Current (ACC), respectively. DOM inputs followed a similar pattern as ammonium, suggesting a substantial contribution of allochthonous sources to the dissolved organic carbon (DOC) pool. Terrigenous input appears to be a main source of ammonium and low-bioavailability carbon, which is supported by a statistically highly significant inverse correlation of these parameters with salinity (Garzón-Cardona et al., 2016). On the other side, intriguingly, usually assumed refractory, so-called humic components

* Corresponding author at: Instituto Argentino de Oceanografía (IADO, CONICET-UNS), Bahía Blanca, Argentina.
E-mail address: jgarzoncardona@iado-conicet.gob.ar (J.E. Garzón-Cardona).

https://doi.org/10.1016/j.jmarsys.2023.103893
Received 28 December 2022; Received in revised form 13 March 2023; Accepted 15 April 2023
Available online 20 April 2023

seem to be vital for DOC microbial turnover in the Patagonian shelf (Garzón-Cardona et al., 2021).

In this context, this sector of the Southwesten Atlantic is particularly relevant for the understanding of the main biogeochemical pathways of autochthonous and allochthonous carbon and nitrogen in the southern end of the American continent, due to its hydrographic complexity, high biological productivity, freshwater inputs, and interoceanic connections (Lara et al., 2010; Garzón-Cardona et al., 2019). The Cape Horn Shelf Current transports low-salinity water from the Southeast Chilean Shelf (Acha et al., 2004, 2020; Guihou et al., 2020), and the ACC and its northward flowing branch, the Malvinas Current (Palma et al., 2021), delivers oceanic nutrient-rich Subantarctic Waters (SAW) to the Patagonian shelf (Lara et al., 2010; Paparazzo et al., 2016; Combes and Matano, 2018). Circulation over the Southern Patagonian shelf depends on the local wind forcing, the propagation of tidal waves, freshwater discharges and the influence of the neighboring deep currents (Palma and Matano, 2012; Sabatini et al., 2016; Brun et al., 2020). There are two types of freshwater input in this region. One is related to the direct discharge of continental streams along the coast, where main rivers are the Deseado, Santa Cruz, Coig, and Gallegos. The Santa Cruz River has the largest discharge with an annual mean value of approximately 710 $m^3\ s^{-1}$, and a peak of 1250$m^3\ s^{-1}$ at the end of the austral summer (March) (Sabatini et al., 2004). The second source is related to the inflow of diluted waters from the Magellan Strait (Panella et al., 1991; Palma and Matano, 2012; Brun et al., 2020), Beagle Channel and the Cape Horn Shelf Current (Guihou et al., 2020).

Despite the clear patterns and drivers for nitrate and ammonium distribution described above, nitrogen origin and dynamics in this region are still not well understood. For example, previous studies (Lara et al., 2010) postulated the assumption that rainfall on the SE Pacific could be the source of ammonium ⊖ in the northern Drake Passage. However, more recent investigations (Garzón-Cardona et al., 2016) suggest that continental runoff rather than wet deposition is an important source of ammonium and DOM in the Pacific-Atlantic connection. Besides the complexities of ammonium dynamics in this region, virtually nothing is known about nitrite (Paparazzo et al., 2010) origin, dynamics and distribution patterns. Some elevated values around 0.8 μM have been reported by Almandoz et al. (2007) in late summer, however no explanation was attempted for these high concentrations, which might be the result of nutrient regeneration in the phytoplankton senescence phase and/or induced by physical processes. We hypothesize that the understanding of regional DIN and DOM connections in these latitudes would benefit from further deepening into the knowledge of seawater optical properties as proxies of DOM freshness and biological activity, synoptically integrated with circulation patterns.

In previous work (Garzón-Cardona et al., 2016, 2019) we investigated the effects of the Pacific-Atlantic connection on nutrient and DOM distributions in the southernmost sector of the Patagonian shelf. From samples taken in 2012 in a larger area, we focused the analysis on the subset south of the Le Maire Strait in an attempt to identify individual influences from the Beagle Channel, North Drake Passage and the Cape Horn Shelf Current. The remaining sampled sector between Le Maire Strait and Grande Bay (Fig. 1), likely containing additional signals from the Magellan Strait, Southern Patagonia rivers and regional circulation patterns, was therefore not included in the analysis. Preliminary screening of data from that sector indicated distribution patterns of nutrients, particularly nitrite, and DOM optical properties that were seemingly influenced by other regional and local processes beyond the scope of the cited works.

Therefore, the general objective of this study is to extend previous investigations in the Beagle Channel and northern Drake Passage sectors (Lara et al., 2010; Sabatini et al., 2016; Barrera et al., 2017; Garzón-Cardona et al., 2016, 2019), expanding the study area to the aforementioned sector north of Le Maire Strait. In particular, the analysis focuses on the role of ACC and freshwater as regional main sources of nutrients and DOC, and the distribution and properties of DIN and DOM in the Southern Patagonian shelf in relation to circulation patterns and seawater optical properties. Previous knowledge about DOM properties in the Pacific-Atlantic connection (Garzón-Cardona et al., 2019) was further developed aiming at a better understanding of relationships among the sources, freshness, humification degree, and chemical nature of DOM, emphasizing its possible role as proxy of biological activity in

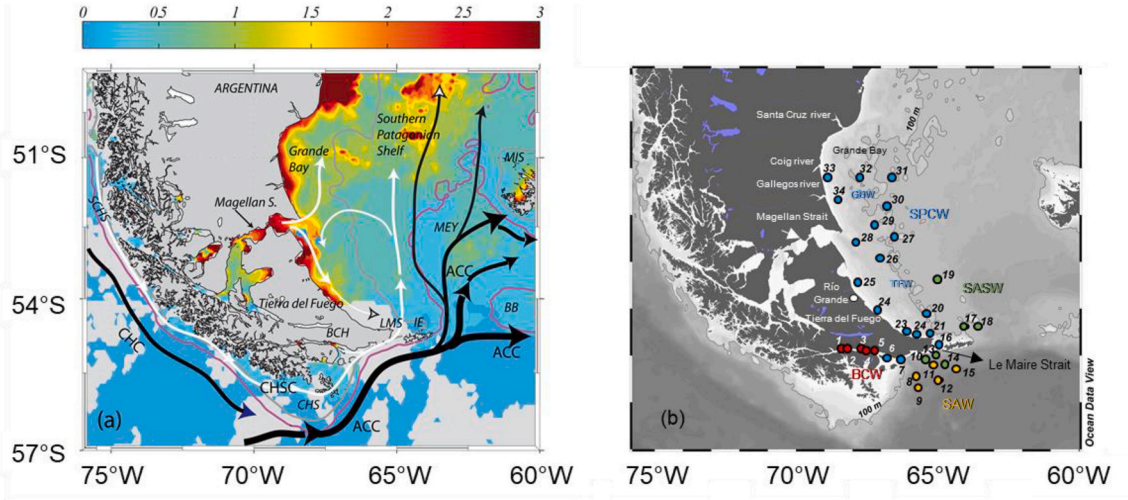

Fig. 1. Geographical setting. (a) Satellite surface Chl-*a* concentration (mg m^{-3}) derived from MODIS 8-day average (29 March-5 April 2012) over the southern tip of South America. Spatial resolution is 9 km. The light gray and magenta lines indicate the 100 m and 200 m isobaths respectively. Black curved lines indicate the approximate direction of the deep ocean flow (CHC: Cape Horn Current, ACC: Antarctic Circumpolar Current). White lines and thin black lines are representative of shelf inflow into the Southern Patagonian Shelf and regional circulation patterns. (SCHS: Southern Chilean Shelf; CHS: Cape Horn Shelf, LMS: Le Maire Strait, IE: Isla de los Estados; MEY: Malvinas Embayment; BB: Burdwood Bank; MIS: Malvinas Islands Shelf, CHSC: Cape Horn Shelf Current). The schematic diagram is based on hydrographic observations and model results (Piola and Gordon, 1989; Palma et al., 2008; Matano et al., 2019; Guihou et al., 2020; Palma et al., 2021). (b) Location of surface sampling stations from 29 March-29 to April 7, 2012 (late summer). Beagle Channel Waters (BCW, red dots), Subantarctic Water (SAW, yellow dots), Subantarctic Shelf Waters (SASW, green dots) and Southern Patagonia Coastal Waters (SPCW, blue dots):Grande Bay Waters (GBW\) and Tierra del Fuego Waters (TFW,). For water type classification, see Section 3.1. Hydrography. (For interpretation of the references to colour in this figure legend, the reader is referred to the web version of this article.)

connection to nitrite maxima. In addition, for the first time in this region, the impact of the regional circulation on physical and chemical properties distribution was studied by means of a regional ocean numerical model and a particle-tracking algorithm.

2. Materials and methods

2.1. Study area and sampling

Sampling was carried out in 2012 during austral late summer/early autumn from March 27 to April 7 at 34 stations distributed in two sectors between 63.55°–68.90°W and 51.20°–55.70°S (Fig. 1). One sector is limited by the Beagle Channel, Le Maire Strait and north sector of the Drake Passage, embracing sixteen stations (Sta 1–16) (Garzón-Cardona et al., 2016, 2019; Barrera et al., 2017). The second one is located between Le Maire Strait and Grande Bay, with nineteen stations (Sta.17–34).

Surface (10 m depth) water samples for inorganic nutrients, DOC and FDOM were filtered immediately after collection through Whatman GF/F glass fiber filters pre-combusted at 450 °C for 4 h (Lara et al., 2010). Each filtrate was split into three aliquots. Samples for inorganic nutrients were stored in alkali-rinsed (0.1 M NaOH) polyethylene bottles. Aliquots for DOC were collected in pre-combusted 20 mL glass vials and acidified to pH < 2 with H_3PO_4. Samples for analysis of fluorescent DOM (FDOM) were collected in pre-combusted 10 mL glass vials. Suspended particulate matter collected on glass fiber filters was used for determination of chlorophyll *a* (Chl-*a*) and phaeopigments. All samples were preserved at −20 °C. Although freezing could potentially alter the structure of some DOM compounds, recent studies have reported minimal changes in DOM due to storage (Hanckel et al., 2014; Sánchez-Pérez et al., 2020; Li et al., 2020).

For logistic reasons, only surface sampling was conducted. Consequently, the dynamics of some of the variables in the shallower stations could be infiuenced to some extent by processes that introduce vertical variability, such as sediment resuspension.

2.2. Pigments analysis

Pigment extraction on duplicate filter samples was performed in 10 mL 90% acetone during 24 h at 4 °C in darkness. Chl-*a* and phaeopigments were quantified by fluorometry, and concentrations were estimated after Holm-Hansen et al. (1965). A standard of pure Chl-*a* (*Anacystis nidulans*) and a Shimadzu RF-5301 fluorometer at λEx/λEm: 460/671 nm were used. The correction for phaeopigments was made by acidification with 0.1 N HCl.

2.3. Inorganic nutrients

Nitrate, nitrite, ammonium, silicate and phosphate (all in μM) were measured using an autoanalyzer (Evolution III, Alliance Instruments) following standard seawater methods (Kattner and Becker, 1991; Grasshoff et al., 1999). The detection limits for nitrate, nitrite, ammonium, silicate and phosphate were 0.10, 0.02, 0.01, 0.05 and 0.01 μM, respectively.

2.4. Dissolved organic carbon

After acidification, duplicate filtrates were analyzed for DOC by high temperature (680 °C) catalytic (Al_2O_3 particles containing 0.5% Pt) oxidation in a TOC analyzer (TOC-VCPN, Shimadzu) followed by quantification of CO_2 by non-dispersive linearized infrared gas analysis (Skoog et al., 1997). A solution of potassium hydrogen phthalate was used as calibration standard.

2.5. Fluorescent dissolved organic matter and indices

Spectral properties of FDOM were determined with a Shimadzu RF-5301 spectrofluorometer with a 150 W xenon lamp and a 1 cm quartz cell. Ultrapure water was used as reference and the intensity of the Raman peak was regularly checked. An estimation of dissolved humic-like components was carried out at the wavelengths proposed by Coble (1996) as follows. Humic-like fluorophores: $FDOM_C$, containing mostly highly unsaturated components, at Ex/Em: 350/440 nm and $FDOM_M$, with low degree of unsaturation, at Ex/Em: 310/380 nm. Absorbance was measured to evaluate the need for correction by internal filter effect. Since values <0.02 were obtained for all the samples with a 1 cm optical path, such a correction was not necessary (Stedmon and Bro, 2008; Murphy et al., 2010). The results were expressed in quinine sulphate equivalent units (QSU), converted with the signal at Ex/Em: 350/451 nm of quinine sulphate dihydrate standard dissolved in 0.05 mol L^{-1} H_2SO_4 and the equivalence 1 QSU = 1 μg L^{-1} (Coble, 1996).

Three indices were used to assess possible sources and diagenetic state of the DOM (Coble, 1996). The fluorescence index (FI) can be used to differentiate DOM origins. FI values ≤1.4 correspond to terrestrially derived DOM, while values ≥1.9 refer to aquatic sources. If FI is between 1.4 and 1.9, DOM components are likely affected by both terrestrial and marine inputs (McKnight et al., 2001). The following formula was used to calculate the fluorescence index: FI = I370/450 / I370/500, where I370/450 represents the fluorescence intensity at Ex/Em: 370/450 nm and I370/500 is the intensity at Ex/Em: 370/500 nm.

The humification index (HIX) is used to assess DOM diagenetic condition and was calculated as the ratio of the areas quantified between emission wavelengths of 435 to 480 nm and 300 to 345 nm for excitation at 254 nm (Zsolnay et al., 1999). HIX increases with the degree of aromaticity as result of a shift in maximum fluorescence intensity from shorter to longer wavelengths associated with an increasing number of highly substituted aromatic nuclei and/or with conjugated unsaturated systems of high molecular weight (Senesi et al., 1991). For example, a HIX value ≥0.9 indicates a high degree of DOM humification (Hansen et al., 2016).

The biological activity index (BIX) can be used to estimate the relative contribution of in-situ produced DOM (Huguet et al., 2009). Values >0.8 indicate that DOM is mainly derived from microbial and other biological sources, whereas those <0.6 indicate a low amount of fresh DOM. BIX is calculated as the ratio BIX = I310/380 / I310/430, where I310/380 is the fluorescence intensity at Ex/Em: 310/380 nm and I310/430 is the fluorescence intensity at Ex/Em: 310/430 nm.

2.6. Numerical Ocean model and particle tracking

To help understand the nutrients distribution in the study area we employed the results of a regional ocean numerical model and a particle tracking algorithm. The regional model configuration extends from 60° S to 40° S in latitude and 81° W to 52.5° W in longitude at 1/12 degree horizontal resolution and 40 terrain-following coordinates in the vertical. The model is nested towards a lower resolution southern hemisphere model at the open boundaries and forced at the surface by daily ERA-Interim winds (Dee et al., 2011) and heat and freshwater fluxes from the Comprehensive Ocean-Atmosphere Data Set (COADS). The main eight tidal constituents are also included. The time integration covers 37 years (1979–2015). For more details about the model development and its validation against in-situ and satellite data the reader is referred to Combes and Matano (2014, 2018, 2019); Matano et al. (2014), Strub et al. (2015), Guihou et al. (2020) and references therein. In this study 10-day averaged values of the model fields for March 2012 were used. To evaluate the impact of the regional circulation on physical and chemical properties distribution we released 14,000 neutrally buoyant floats at specific locations and from surface to bottom at the beginning of January and followed their trajectories during 90 days. The floats

trajectories were calculated offline using the 3-D velocity field from the regional ocean model employing the algorithm described in Batchelder (2006). Relative concentrations were computed at the end of simulation time using the particle's final position (Palma et al., 2021).

2.7. Statistical analysis

The relationships among optical signatures of DOM, inorganic nutrients and hydrographic parameters were assessed with the software PAST 2.17c (Hammer et al., 2001). Parametric Pearson's rank correlation was applied, and the degree of significance was termed: not significant ($p > 0.05$), significant ($0.05 < p > 0.01$) or highly significant ($p \leq 0.001$).

3. Results and discussion

3.1. Hydrography

A temperature–salinity (T – S) diagram (Fig. 2) allowed the identification of four water masses in the study area:

1) Waters of the Beagle Channel (BCW), with temperatures between 7.9° and 8.9 °C, low salinities (29.3–31.2) and depths between 20 and 50 m. These characteristics were associated with those of the Cape Horn Shelf Current, with temperatures >7 °C and salinities <34.0 due to a high precipitation regime in the zone of the Chilean fjords and ice melting in Southern Patagonia (Guihou et al., 2020; Giesecke et al., 2021; Iachetti et al., 2021).

(2) Subantarctic Water (SAW), with high salinities (> 34.0) and depths (1093–2285 m) and low temperatures (< 6.4 °C) (Fig. 2), derived from the Northern Drake Passage (Piola and Gordon, 1989; Matano et al., 2019).

(3) Subantarctic Shelf Water (SASW), from the external BCW to the Grande Bay, with warmer and saline water in the eastern part of Patagonian shelf, temperatures, salinities and depths ranging 7.6° -8.5 °C, 33.2–33.8, and 115–1783 m, respectively. The wide ranges of depths, salinity and temperature in the SASW point to the connection and transition among the water masses from the Magellan Strait and the Antarctic Circumpolar Current (ACC) (Guihou et al., 2020; Brun et al., 2020).

4) Southern Patagonia Coastal Waters (SPCW) (Guerrero and Piola, 1997), located at depths below 100 m (Fig. 1b) and embracing Grande Bay waters (GBW) north of the Magellan Strait mouth and the coastal waters off Tierra del Fuego (TFW) in the south (Fig. 1b). These water masses have salinities lower than 33.4 and are influenced by outflow from the Magellan Strait and small riverine discharges attached to the coast in Grande Bay (Palma and Matano, 2012; Brun et al., 2020), and are composed by a mix of Cape Horn Shelf waters, BCW and SASW intruding the Patagonian Shelf mainly through Le Maire Strait in the coastal region off Tierra del Fuego (Guihou et al., 2020; Brun et al., 2020). Surface temperatures lay between 8.4° and 9.7 °C with lower values near and offshore the Magellan Strait mouth and higher values close to the coast (Fig. 2).

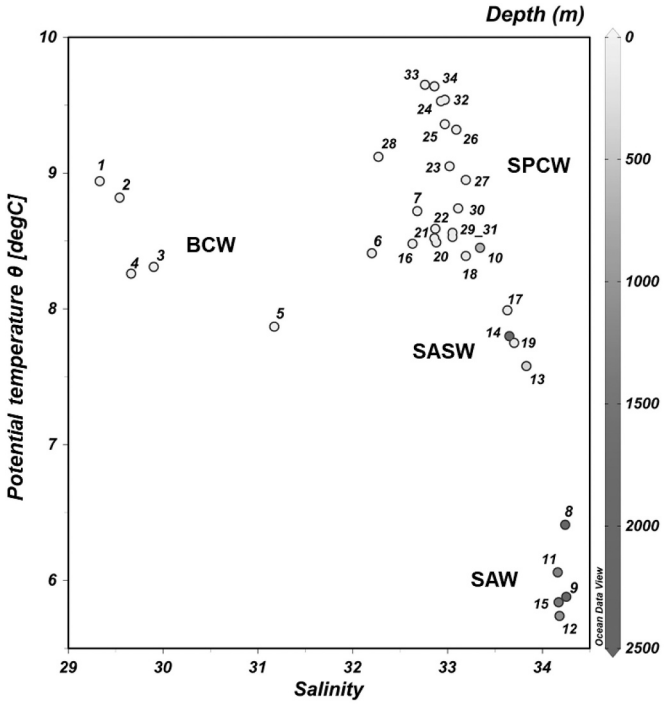

Fig. 2. Division of the study area in four water types based on surface temperature and salinity, as well as bathymetric data. Abbreviation: Beagle Channel Water (BCW), Subantarctic Water (SAW), Subantarctic Shelf Water (SASW) and Southern Patagonia Coastal Water (SPCW).

3.2. Distribution and relationship between inorganic nutrients, salinity, temperature, circulation patterns and biological activity

3.2.1. Nutrients and salinity

Surface concentrations of nitrate, phosphate and silicate (Fig. 3C, D, G) showed a clear gradient with highest concentrations in SAW and lowest values in SPCW. In SASW and SAW, these nutrients presented a decreasing trend from SE to NW. In general, these trends can be ascribed to the transport of nutrient-rich water from the ACC to shelf waters (Palma et al., 2021).

However, surface concentrations of these nutrients presented a distinct characteristic in SPCW. Mainly phosphate and silicate appear to have additional sources. Relatively high concentrations of both in the GBW and TFW sectors of SPCW could be related to increased regeneration due to longer residence times as shown in the particle model (Fig. 4b). The shape of these two sectors, with a low-concentration area between them, suggests a modest contribution of these nutrients by the Magellan Strait. Further, nitrate is low from the mouth of the Magellan Strait to GBW, with an intrusion of high-salinity (Fig. 3A), high-nitrate (Fig. 3C), low-ammonium (Fig. 3F) water from SASW reaching the Rio Grande coastal sector of TFW (see also Fig. 1). The concentrations of nitrate, phosphate and silicate in BCW were similar to those reported by Giesecke et al. (2021). Yet, their silicate values were somewhat higher (5–6 μM), probably because their sampling was carried out in winter and planktonic Si uptake was low.

From these nutrients, those with a source of likely predominantly ACC origin show strong positive correlations with salinity (Fig. 5). Nitrate and phosphate showed the highest correlations, with $r = 0.79$, and $r = 0.83$, $n = 34$, $p < 0.001$, respectively (Fig. 5A and B). Despite the highly significant correlation of the linear regression between nitrate and salinity, an exponential fit ($y = 7.76 + \exp.[0.88\ (x\text{-}31.41)]$ renders a much higher $r = 0.96$. This nonlinear relationship between both variables could be due to recent and on-going nitrate uptake. In BCW, where Chl-a values are highest, nitrate seems independent of salinity variation at values ≤32, probably due to on-going uptake, while in most other sectors, low Chl-*a* and high phaeopigment values point to a declining phytoplankton activity and grazing. The correlation of silicate and salinity was also positive albeit weaker, with $r = 0.42$, $p < 0.05$ (Fig. 5D). This supports the assumption above of a secondary source of continental origin for silicate, which would increase data scatter and reduce positive correlation through freshwater nutrient input. Additionally, its much lower concentration of more than an order of magnitude as compared to nitrate, likely brings in further variability derived from siliceous phytoplankton uptake following Redfield-Brzezinski ratios C:Si:N:*P* = 106:15:16:1 (Brzezinski, 1985). A further possible silicate source could be related to sediment resuspension and resulting interstitial pore water fluxes in the shallower sectors.

In contrast to the nutrients discussed above, the relationship between

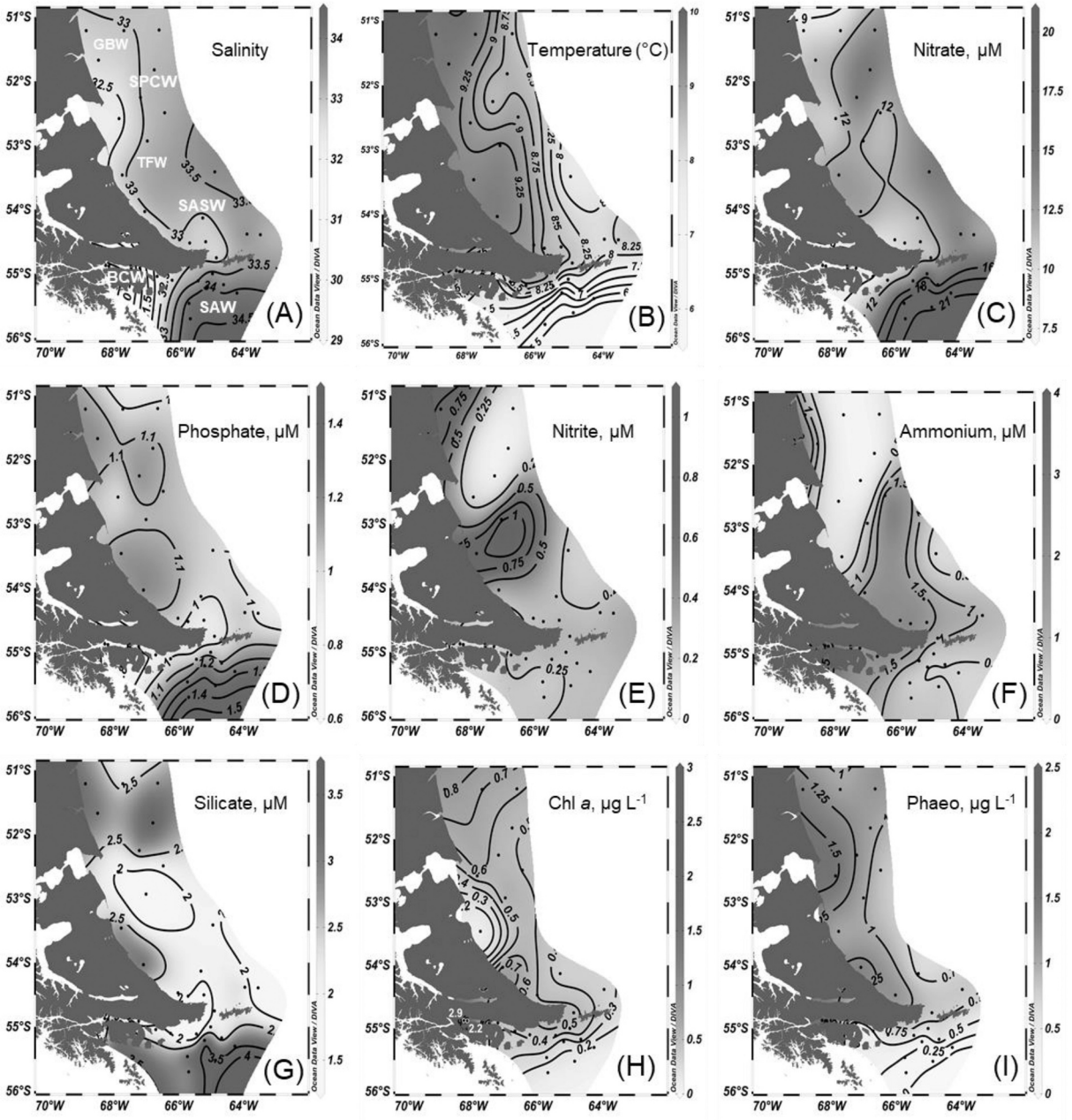

Fig. 3. Surface distribution of temperature, salinity, inorganic nutrients and photosynthetic pigments (Chl-*a*: chlorophyll a, Phaeo: phaeopigments).

ammonium and salinity (Fig. 5C) shows a strongly negative, highly significant correlation ($r = -0.74$, $n = 34$, $p < 0.001$).

This, together with the distribution pattern of higher concentrations associated with the BCW (Fig. 3F), point to freshwater sources of ammonium in Tierra del Fuego related to stream inputs, lixiviation from fjords and peatlands, melting glaciers and the inflow of waters from the Southern Chilean Shelf and Cape Horn Shelf current through the Le Maire Strait (Guihou et al., 2020; Palma et al., 2021).

3.2.2. *Nutrients and temperature*

Most nutrients do not show a direct relationship to temperature, excepting that arising from the origin of the water mass, notably as in the case of the cold, nutrient-rich ACC and nitrate, which is better expressed by its salinity. An exception seems to be the behavior of nitrite. Besides the evident dependence of nutrient concentration on salinity (Fig. 5A, B, C, D), their increased variability at a salinity of about 33 is noteworthy, and particularly accentuated for nitrite (Fig. 5E). This nutrient presents a distinct behavior, evidenced by a particular distribution pattern without any obvious relationship to the potential hydrographic sources described above, only sharing with the other nutrients the high variability in the SPCW. In this sector, nitrite reaches concentrations of 1.1 µM (see Table 1), to our knowledge the highest reported in the Southwesten Atlantic, with a core of above-average concentrations ranging 0.6–1.1 µM in TWF and to a less extent in GBW (Fig. 3E) and that occurs at water temperatures in the quintile of highest registered values (9.0–9.7 °C) (Fig. 3B and 5F) and salinities around 33 (Fig. 3A and 5E). This particular setting can be clearly visualized in a contour plot of nitrite against with temperature and salinity (Fig. 5G).

3.2.3. *Nutrients and circulation patterns*

The distributions of nitrate and ammonium (Fig. 3C and F) seem to roughly delimit the reaches of a high-nitrite sector (Fig. 3E). This may have two non-excluding reasons. On the one side, they could be

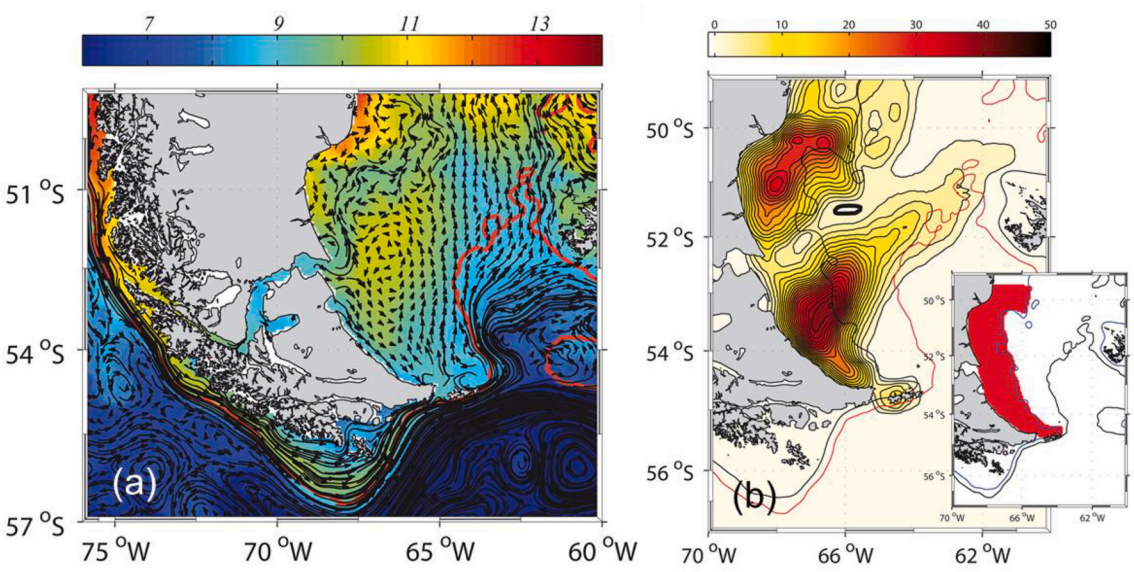

Fig. 4. Circulation and retention patterns. (a) Sea surface temperature (colors) and depth-averaged velocity vectors from March 24 to April 3, 2012 (10-day averaged) computed from a numerical model (Combes and Matano, 2018). The red line is the 200 m isobath. (b) Particle's relative concentration scaled with respecto to its initial value (%) 90 days after release in January 1st 2012. The black line is the 100 m isobath. The particle's release area is indicated in the inset (inside the 100 isobath). (For interpretation of the references to colour in this figure legend, the reader is referred to the web version of this article.)

considered to be representative of local circulation patterns (see below) of ammonium-rich BCW and nitrate-rich water from the SASW, respectively intruding and protruding into SPCW and physically confining the extension of the high-nitrite core. On the other side, these nutrients could be respectively acting as substrate for denitrification or more likely nitrification, fueling nitrite production by bacterial activity (Zakem et al., 2018), what will be discussed in section 3.2.4.

The possibility of a physical delimitation of the high-nitrite sector could be supported by local recirculation patterns that have been postulated for the region, particularly an anticyclonic cell (Fig. 4a) driven by the combined action of local winds and tidal forcing (Palma et al., 2008). In this context, the catalyzing effect of local frontal activity, as well as eventual vertical nutrient and DOM fluxes from particle resuspension in the shallower sectors cannot be ruled out and deserve, together with the distinctive nitrogen dynamics in this region, further investigation.

Further, an increased biological activity in SPCW could also be favored by longer residence times and elevated concentrations of suspended particulate organic matter. This assumption is strongly sustained by the concentration patterns (Fig. 4b) obtained from the particle tracking algorithm fed with the 10-day averaged 3D velocity from the summer 2012, showing two cores of high particle relative concentration (%) in GBW and TFW respectively. Particularly the core in TFW shows a maximum in long-term (at least 90 days) particle retention at the same location as the nitrite maximum.

3.2.4. Nutrients and biological activity

The assumption of nitrite production by elevated biological activity is supported by the spatial distribution of high values of BIX, which reaches values >0.6 combined with temperatures >9 °C in the high-nitrite sectors (contour plot in Fig. 5H). These high BIX values could be related to a setting of nutrient regeneration during phytoplankton senescence, as shown in Fig. 8C, where BIX > 0.6 occur at high phaeopigment concentrations (> 0.5 μg L^{-1}). Additionally, high bacteria counts in this sector have been reported by Krock et al. (2015) for the same cruise. In their Fig. 5, between 50°- 53°S the stations with highest abundance of heterotrophic bacteria (HB), ranging 1.3–1.9 10^6 cells mL^{-1}, coincide with the corresponding ones with high nitrite values in the range 0.6–1.1 μM. In the remaining stations of this area, HB abundance was ≤1.0 10^6 cells mL^{-1}.

Regarding the likely situation of phytoplankton senescence discussed above, Garzón-Cardona et al. (2016) reported that the concentration of Chl-*a* showed a decreasing tendency from the east of the Beagle Channel to the west of Tierra del Fuego region. The horizontal distribution of Chl-*a* is shown in Fig. 3H, which illustrates declining values from inshore to offshore sites. High Chl-*a* concentrations were found only at two stations in BCW (2.9 and 2.2 μg L^{-1}). Values were similar to those reported by Iachetti et al. (2021) and Giesecke et al. (2021), but lower than in Guinder et al. (2020). In the area located between the Le Maire Strait and Grande Bay the concentrations of Chl-*a* fluctuated from 0.8 μg L^{-1} to 0.1 μg L^{-1}. In SASW the highest value was 0.5 μg L^{-1}, gradually decreasing to a range of 0.1–0.3 μg L^{-1} in SAW (Fig. 3H). In the SPCW the highest Chl-*a* concentrations occurred in GBW, decreasing towards the mouth of the Magellan Strait, reaching a minimum in the north sector of TFW and increasing again to the south. Late-summer recent and remnant autotrophic uptake is likely a reason for the nonlinear relationship between nitrate and salinity and the weaker correlation between silicate and salinity. Phaeopigment concentrations (Fig. 3I) followed a similar pattern as Chl-*a*, yet with mostly higher values, and maxima in the Grande Bay zone extending south of the Magellan Strait mouth, depicting a situation of seasonal phytoplankton senescence typical for this region (Sabatini et al., 2016).

3.3. Sources and main features of DOC, humic DOM, and the fluorescence index

3.3.1. DOC and humic DOM

The concentrations of DOC and intensities of the DOM humic components $FDOM_C$ and $FDOM_M$ (Table 1) are within the range previously observed in SAW (Garzón-Cardona et al., 2019, 2021). DOC is generally low, even in the high-concentration sector in BCW, where it reaches a maximum of only 77 μM C, despite evidence of terrestrial input as discussed for ammonium. Synoptically, it is noteworthy that high DOC, $FDOM_C$ and $FDOM_M$ values and their increasing gradient towards the coast (Fig. 6A and B, only $FDOM_C$ is shown for its similarity with $FDOM_M$) approximately follow the distribution of salinities <33 (Fig. 3A), besides reflecting the effect of the intrusion of saltier, DOC-poorer waters of the SAW and SASW. In more detail, the humic-like

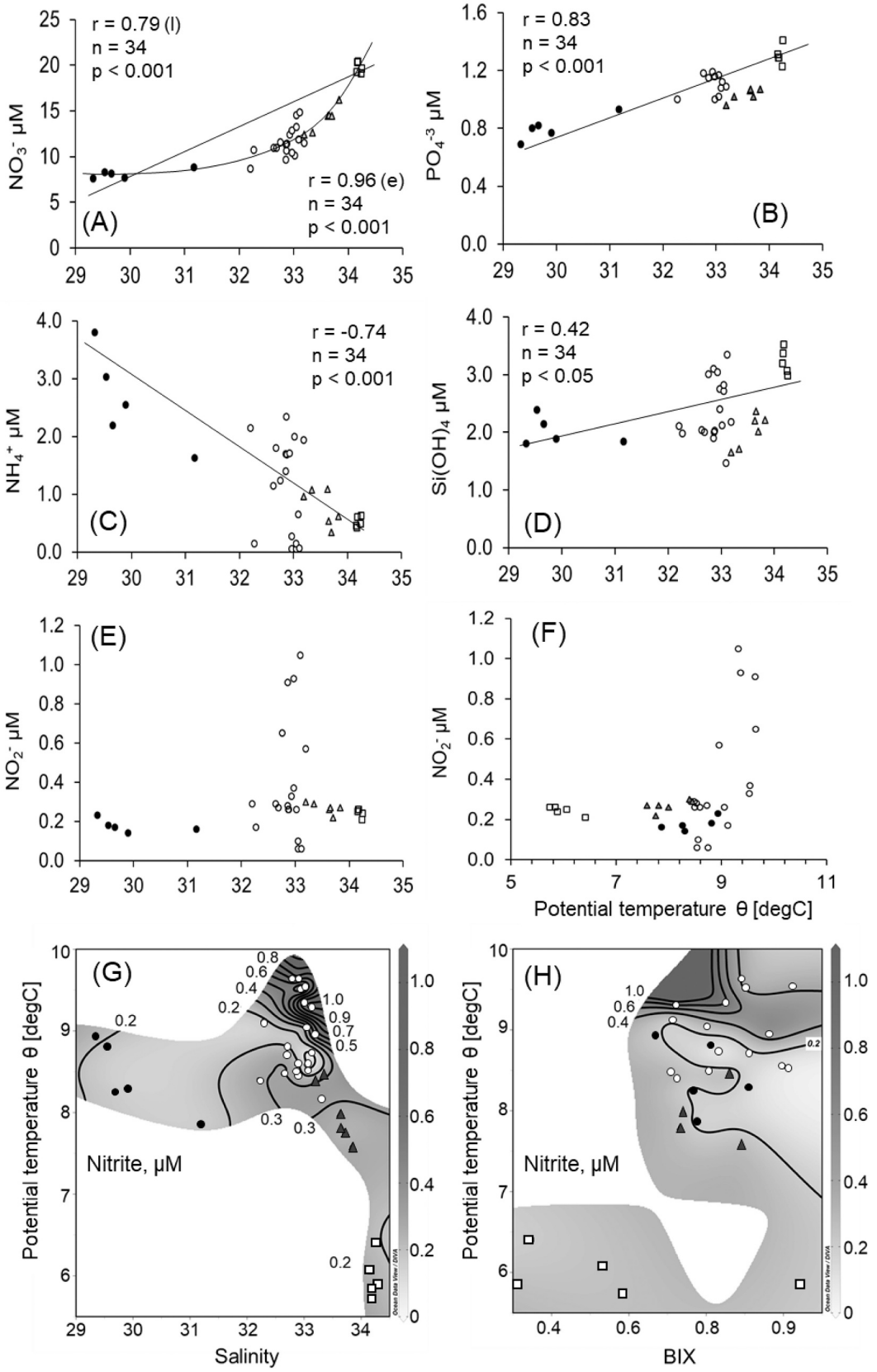

Fig. 5. General relationship of nutrients with salinity and specifically of nitrite against temperature, salinity and biological activity index (BIX). Water type symbols: white circles (SPCW), black circles (BCW), triangles (SASW), squares (SAW). In Fig. 5A, l = linear, e = exponential.

Table 1
Data obtained in different sectors of the eastern study region. Average, ±standard deviations and ranges [:] of depth (m), temperature (°C), salinity, dissolved inorganic nutrients (in μM: NO_3^-, nitrate, NO_2^-, nitrite, $Si(OH)_4$, silicate, PO_4^{-3}, phosphate, NH_4^+, ammonium). Dissolved organic carbon (DOC, μM C)). Fluorescent dissolved organic matter intensities (in QSU): Humic-like components: $FDOM_C$ (highly unsaturated), $FDOM_M$, (low degree of unsaturation). Indices: HIX (humification index), FI (fluorescence index), BIX (biological activity index): pigments (in μg L^{-1}): Chl-*a* (chlorophyll *a*), Phaeo (phaeopigments). Water types: BCW (Beagle Channel), SAW (Subantarctic), SASW (Subantarctic Shelf) and SPCW (Southern Patagonia Coastal Waters). n = number of samples.

Variable	BCW	SAW	SASW	SPCW
Depth	38 ± 12	1651 ± 553	527 ± 647	73 ± 29
(n = 34)	[20:50]	[1093:2285]	[115:1783]	[29:119]
Temperature	8.4 ± 0.4	6.0 ± 0.3	8.0 ± 0.4	9.0 ± 0.5
(n = 34)	[7.9:8.9]	[5.7:6.4]	[7.6:8.5]	[8.4:9.7]
Salinity	29.9 ± 0.7	34.2 ± 0.1	33.6 ± 0.2	32.9 ± 0.3
(n = 34)	[29.3:31.2]	[34.2:34.3]	[33.2:33.8]	[32.3:33.2]
NO_3^-	8.1 ± 0.5	19.8 ± 0.6	14.1 ± 1.4	11.5 ± 1.6
(n = 34)	[7.6:8.8]	[19.1:20.4]	[12.4:16.2]	[8.7:14.8]
NO_2^-	0.2 ± 0.0	0.2 ± 0.1	0.3 ± 0.1	0.4 ± 0.3
(n = 34)	[0.1:0.2]	[0.2:0.3]	[0.2:0.3]	[0.1:1.1]
$Si(OH)_4$	2.0 ± 0.3	3.2 ± 0.2	2.0 ± 0.3	2.4 ± 0.5
(n = 34)	[1.8:2.4]	[3.0:3.5]	[1.7:2.4]	[1.5:3.4]
PO_4^{-3}	0.8 ± 0.1	1.3 ± 0.1	1.0 ± 0.1	1.1 ± 0.1
(n = 34)	[0.7:0.9]	[1.2:1.4]	[1.0:1.1]	[0.9:1.2]
NH_4^+	2.6 ± 0.8	0.5 ± 0.1	0.8 ± 0.3	1.1 ± 0.8
(n = 34)	[1.6:3.8]	[0.4:0.6]	[0.3:1.1]	[0.1:2.3]
DOC	67.8 ± 5.8	54.1 ± 5.3	54.8 ± 5.5	64.6 ± 5.5
(n = 34)	[62.7:77.0]	[46.0:58.7]	[48.9:63.9]	[51.7:73.2]
$FDOM_C$	1.1 ± 0.2	0.3 ± 0.1	0.3 ± 0.1	0.7 ± 0.2
(n = 29)	[0.8:1.4]	[0.2:0.4]	[0.2:0.5]	[0.4:1.0]
$FDOM_M$	1.1 ± 0.3	0.3 ± 0.1	1.6 ± 1.2	0.7 ± 0.2
(n = 29)	[0.8:1.5]	[0.2:0.4]	[0.7:3.3]	[0.3:1.0]
HIX	1.7 ± 0.3	0.7 ± 0.4	0.8 ± 0.2	1.3 ± 0.3
(n = 29)	[1.1:2.0]	[0.3:1.3]	[0.6:1.0]	[0.8:1.8]
FI	1.7 ± 0.2	3.6 ± 0.6	3.2 ± 0.2	2.4 ± 0.3
(n = 29)	[1.5:1.9]	[3.0:4.3]	[3.0:3.4]	[1.7:2.9]
BIX	0.8 ± 0.1	0.5 ± 0.1	0.8 ± 0.1	0.9 ± 0.1
(n = 29)	[0.7:0.9]	[0.3:0.6]	[0.7:0.9]	[0.7:1.0]
Chl-*a*	1.3 ± 1.2	0.2 ± 0.1	0.4 ± 0.1	0.5 ± 0.2
(n = 29)	[0.3:2.9]	[0.1:0.3]	[0.3:0.5]	[0.1:0.8]
Phaeo	1.0 ± 0.5	0.2 ± 0.1	0.7 ± 0.1	1.0 ± 0.3
(n = 29)	[0.5:2.3]	[0.1:0.2]	[0.6:0.8]	[0.5:1.6]

components showed analogous distribution patterns, with high values in BCW and MSW (0.4–1.4 QSU), and marked decreases to <0.4 QSU at the more marine stations (SASW and SAW) (Fig. 6B). $FDOM_C$ and $FDOM_M$ intensities positively correlated with each other ($r = 0.94$, $p < 0.001$, $n = 29$), and showed a highly significant negative correlation with salinity ($FDOM_C$, $r = 0.83$; $FDOM_M$, $r = 0.78$; $p < 0.001$, $n = 29$, Fig. 7C and D, respectively), suggesting that both have a common origin in the freshwater input into the southernmost sector of the Patagonian Shelf.

Interestingly, a lower, yet still significant positive correlation was also obtained between humic-like components and Chl-a ($FDOM_C$, $r = 0.66$; $FDOM_M$, $r = 0.68$). Correlations with phaeopigments was also positive but lower ($FDOM_C$, $r = 0.50$; $FDOM_M$, $r = 0.47$). Although previous studies have also found that multiple terrestrial humic-like components can show similar biogeochemical behaviors along aquatic gradients in a determined region (Gonçalves-Araujo et al., 2015; Zhou et al., 2019), $FDOM_C$ and $FDOM_M$ do very likely correspond to chemically distinct DOM fractions. $FDOM_C$ is associated with highly degraded terrigenous humic material, while $FDOM_M$ is conventionally assigned as a marine humic-like component, and thought to be generated by heterotrophic reprocessing of aquatic autochthonous DOM (Coble, 1996; Cabrera-Brufau et al., 2022). Yet, in our study, there is a much higher correlation between these peaks intensities and salinity as tracer or terrigenous input than with proxies of biological activity such as chlorophyll or phaeopigments.

$FDOM_C$ correlates slightly better with salinity than $FDOM_M$, and this in turn correlates better with chlorophyll than $FDOM_C$ does. It could be inferred that $FDOM_M$ was only moderately associated with aquatic primary production. This could be caused by several factors: Chl-*a* was mostly low across our study region, so there simply might not have been enough variation in aquatic primary production to produce a higher correlation. Additionally, $FDOM_M$ probably has a main terrestrial source from Fuegian peatlands, without discarding that a fraction corresponds to microbially reprocessed DOM, as suggested by other studies (Murphy et al., 2008; Yamashita et al., 2017). Nevertheless, crossed correlations are possible. For example, the correlation between Chl-*a* and salinity is $r = 0.68$, $p = 0.01$, $n = 29$, which is very similar to that between $FDOM_M$ and Chl-*a*. Thus, without discarding any of the possibilities discussed above, speculation about sources of aquatic humic in compounds in this complex environment requires caution.

3.3.2. *The fluorescence index*

The fluorescence index (FI) can be useful to differentiate DOM origins. FI ranged between 1.5 and 4.3 (Table 1) and its horizontal distribution (Fig. 6C) showed a clear gradient with highest values in SAW and SASW (2.9–4.3) and lowest in BCW and SPCW (1.5–2.9). DOM derived from terrestrial sources (degraded plant and soil organic matter) presents lower FI values than material directly produced by aquatic sources such as extracellular release and leachates from algae and bacteria (McKnight et al., 2001; Hansen et al., 2016). FI values ≤1.4 correspond to terrestrially derived DOM, while those ≥1.9 refer to aquatic sources. If FI is between 1.4 and 1.9, DOM components originate from both, terrestrial and marine sources (McKnight et al., 2001). Hansen et al. (2016) observed that for algae leachates, FI showed large changes over

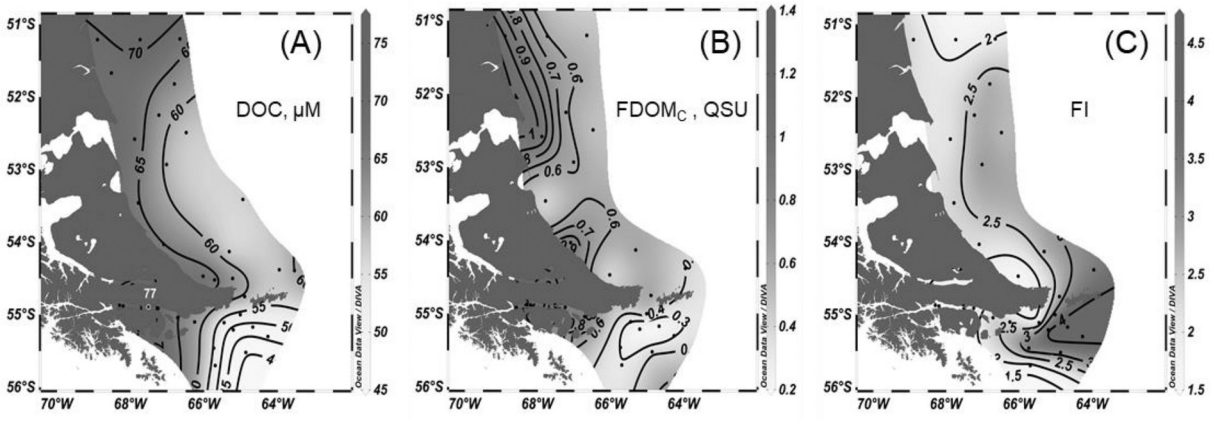

Fig. 6. Distribution of DOC, fluorescent humic-like dissolved organic matter ($FDOM_C$) and fluorescence index (FI) in surface waters of the study zone.

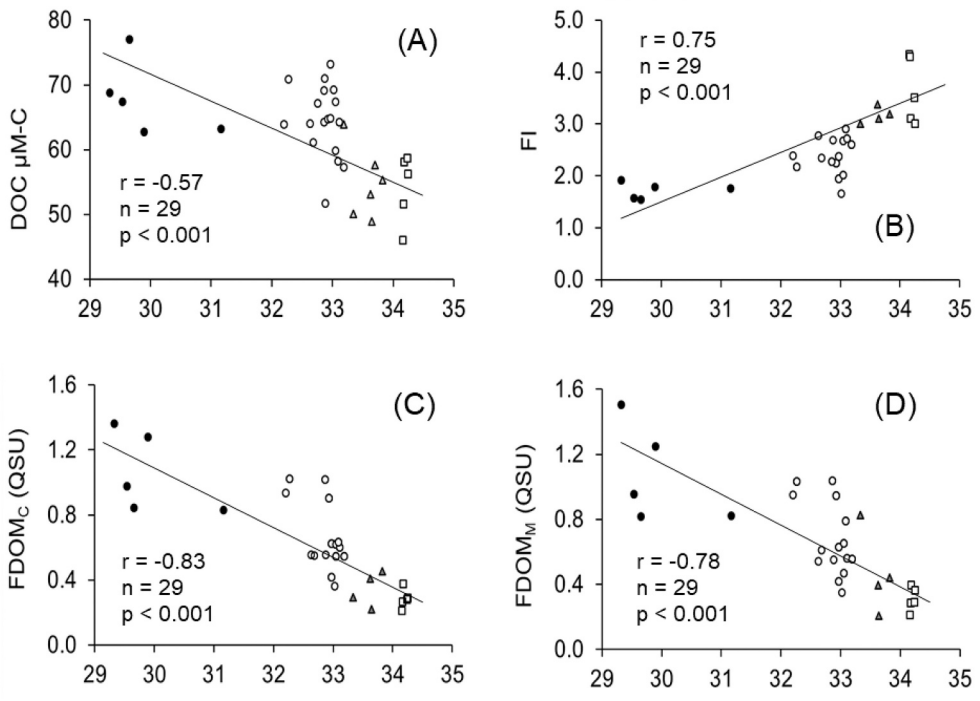

Fig. 7. Relationship of DOC, humic components $FDOM_C$ and $FDOM_M$, and fluorescence index (FI) with salinity. Water type symbols: white circles (SPCW), black circles (BCW), triangles (SASW), squares (SAW).

time, with final values around 3.5, alike those observed in the SAW and SASW zones (Fig. 6C). The lowest values in BCW point to a substantial influence from terrestrial sources in this sector and to a lesser extent in MSW, as also indicated by $FDOM_M$. Highly significant correlations of DOC and FI with salinity, ($r = -0.57$, $p < 0.001$, $r = 0.75$, $p < 0.001$, Fig. 7A and B, respectively) depict the dilution of DOM by mixing with more oceanic, DOC-poor waters and the related shift in DOM composition towards a higher relative contribution from aquatic sources.

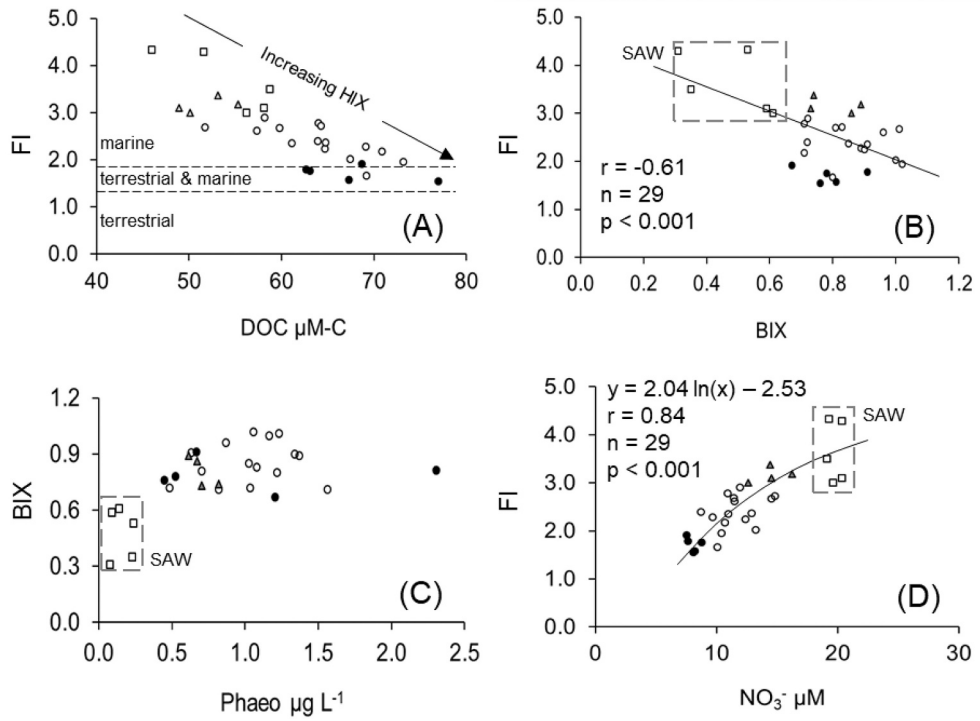

Fig. 8. Relationships between fluorescence (FI) and biological activity (BIX) indices and dissolved organic carbon (DOC), nitrate (NO_3^-) and phaeopigments (Phaeo). Water type symbols: white circles(MSW), black circles (BCW), triangles (SASW), squares (SAW).

3.4. Integrated synthesis of DOC molecular nature, DOM freshness and DIN distribution

3.4.1. Origin and molecular nature of DOC

Despite the narrow range of DOC concentrations (46–77 μM C), the nature of the different DOM sources discussed above is reflected in a highly significant inverse correlation ($r = -0.82$, $n = 29$, $p < 0.001$) between DOC and FI values (Fig. 8A). This further sustains the characterization of DOM in the open Subantarctic waters (SASW and SAW) as mainly originated from planktonic sources, and in the more coastal BCW and SPCW as a mixture of autochthonous and continental components. The trend of the regression line suggests that in the study region, DOC concentrations >80 μM C, can be expected to occur at FI ≤ 1.4 and to be mainly of terrigenic origin. The lowest registered DOC values were close to the concentration of termed refractory background DOC (~38 μM C) resistant to microbial degradation, present throughout the water column in the ocean, and characterized by old material (4000–6000 years according to ^{14}C dating), which likely survives multiple mixing cycles in the ocean (Druffel et al., 1992, 2019). Consistently with this, in our work these low concentrations occur at high FI values, implying a predominantly aliphatic character of DOM, typical of purely marine humic compounds (Ishiwatari, 1992).

Additionally, HIX ranged 0.27–2.02 and showed a highly significant direct correlation with DOC ($r = 0.64$, $n = 29$, $p < 0.001$) indicating a higher aromatic character of DOM components at increasing DOC concentrations (see HIX trend arrow in Fig. 8A). The highest HIX values (> 1) indicate an advanced degree of humification of the peatland-derived DOM components present in seawater (Hansen et al., 2016).

3.4.2. DOM freshness, biological activity and DIN distribution

There is a statistically significant inverse relationship ($r = -0.68$, n = 29, p < 0.001) between the biological activity index BIX (Fig. 8B) and FI, implying a mixture of aliphatic and aromatic DOM components with increasing BIX, and a more aliphatic character ("old" DOM) at low biological activities and high FI, as in SAW. BIX values >0.6, which indicate higher biological activity (see discussion on nitrite above), and hence freshly produced DOM, occur at intermediate to low FI values. This is probably related to the fact that in the study region, higher planktonic activity was detected in BCW and other coastal sectors, where ammonium and DOM of terrestrial origin are high, likely producing a mixture of autochthonous and allochthonous dissolved organic components. The relationship between BIX and autotrophic and heterotrophic activity can be also depicted through the relationship between this index and the concentration of phaeopigments (Fig. 8C). Fresh DOM can also be produced by sloppy feeding of zooplankton on microalgae (Møller, 2007), which would be consistent with the higher phaeopigment values. Again, BIX values <0.6 appear to be related to the high-nutrient-low-chlorophyll SAW (Fig. 3I) (Dugdale and Minas, 1995; Lara et al., 2010; Sabatini et al., 2016), where phaeopigments are low too. BIX values >0.6 mostly occur at higher phaeopigment values (> 0.5), suggesting a setting of higher bacterial activity associated to the senescence of the phytoplankton community in late summer, a condition under which inorganic nitrogen regeneration seems to be taking place mainly in SPCW, as stated before in the nitrite discussion in section 3.2.4.

Also in relation to distribution of inorganic nitrogen, FI revealed to be a good auxiliary tracer of water mass origin and nitrate concentration. Fig. 8D shows the nonlinear relationship between both parameters, with a highly significant correlation ($r = 0.84$, $n = 29$, $p < 0.001$) and the clear delimitation of the high-nitrate SAW, which originates from ACC water, ultimate source of nitrate for much the Southern Ocean. The logarithmic relationship between both variables seems realistic, since FI is not assumed to further increase in ACC, given the almost background DOC concentrations of likely "old" DOM. At a concentration of 36 μM N, considered the signature nitrate concentration of the Upper Circumpolar Deep Water (Sigman et al., 2000), the regression equation predicts a FI value of 4.8, which seems quite realistic at low DOC (see Fig. 8 A).

4. Conclusions

Four different water types were identified, namely BCW, SAW, SASW and SPCW. The latter was divided in two subtypes (TFW and GBW), based on the occurrence of cores with high particle concentration. The surface distribution of inorganic nitrogen nutrients presents distinct characteristics related to their origin: the ACC is the main source of nitrate, while ammonium shows inputs from freshwater sources in Tierra del Fuego and the Cape Horn Shelf Current. Nitrite presents a distribution pattern without any obvious relationship to the above-mentioned sources, with high concentrations in TFW and GBW. Nitrite production is likely driven by elevated bacterial activity, related to a late-summer/early autumn setting of nutrient regeneration and freshly produced DOM during senescence and grazing of the phytoplankton population. Anticyclonic cells with high particle residence times could favor this process. The current work reports for the first time the existence of high nitrite values in this region and postulates a mechanism for their occurrence.

High DOM concentrations roughly follow the distribution of salinities <33. DOC maxima were lower as expected for a region with considerable terrestrial runoff, and minima were close to global background levels. The fact that humic components of DOC, as well as ammonium present a highly significant inverse correlation with salinity, point out that freshwater input is a key source of reduced nitrogen and refractory carbon in this region. Furthermore, the HIX index increases with DOC, suggesting a high aromatic character of terrestrial humic material in BCW, derived from Fuegian peatlands. The fluorescence index FI indicates that DOM in SAW and SASW is mainly of planktonic origin and that in the more coastal BCW and SPCW waters it consists of a mixture of autochthonous and continental components. Low DOC concentrations at high FI values imply a predominantly aliphatic character of that DOM, typical of refractory marine humic components.

Considering the influence of terrestrial runoff on the input of DOM and ammonium in the studied sector, it appears relevant to investigate their regional dynamics during the peak period of freshwater inputs from continental ice melting in spring/early summer (Iturraspe et al., 1989). Complementarily, the confirmation of the postulated formation mechanisms of nitrite high-concentration zones would require additional studies on vertical structure, sediment resuspension, abundance and activity of zooplankton and heterotrophic bacteria.

Declaration of Competing Interest

The authors declare that they have no known competing financial interests or personal relationships that could have appeared to influence the work reported in this paper.

Data availability

Data will be made available on request.

Acknowledgements

We are thankful to the crew of the research vessel BO "Puerto Deseado" for their support during field activities and sampling. We also thank Gustavo A. Lovrich (CADIC), scientific leader of the expedition "Patagonia Austral" on board R/V Puerto Deseado (CONICET-MINDEF). This work was financed by the binational project MINCyT-BMBF (AL/11/03-ARG 11/021) and FONCYT: PICT 0467–2010 to RL. EDP was partially financed by FONCYT: PICT 2020-2024. The DOM sections of this work were written at the Alfred Wegener Institute for Polar and Marine Research, Bremerhaven, as part of the activities funded by a grant from the Alexander von Humboldt Foundation (ARG 1015835 HFST) to RJL and JEGC. We also acknowledge V. Combes for sharing the

outputs of the regional numerical ocean model.

References

Acha, E.M., Mianzan, H.W., Guerrero, R.A., Favero, M., Bava, J., 2004. Marine fronts at the continental shelves of austral South America: physical and ecological processes. J. Mar. Syst. 44, 83–105.

Acha, E.M., Viñas, M.D., Derisio, D., Alemany, D., Piola, A.B., 2020. Large-scale geographic patterns of pelagic copepods in the southwestern South Atlantic. J. Mar. Syst. 204, 103281.

Almandoz, G.O., Ferrario, M.E., Ferreyra, G.A., Schloss, I.R., Esteves, J.L., Paparazzo, F. E., 2007. The genus pseudo-nitzschia (Bacillariophyceae) in continental shelf waters of Argentina (south western Atlantic Ocean, 38–558S). Harmful Algae 6, 93–103.

Barrera, F., Lara, R., Krock, B., Garzón-Cardona, J.E., Fabro, E., Koch, B.P., 2017. Factors influencing the characteristics and distribution or surface organic matter in the Pacific-Atlantic connection. J. Mar. Syst. 175, 36–45.

Batchelder, H.P., 2006. Forward-in-time−/backward-in-time-trajectory (fitt/bitt) modeling of particles and organisms in the coastal ocean. J. Atmos. Ocean. Technol. 23, 727–741.

Brun, A.A., Ramirez, N., Pizarro, O., Piola, A.R., 2020. The role of the Magellan Strait on the southwest South Atlantic shelf. Estuar. Coast. Shelf Sci. 237, 106661.

Brzezinski, Mark A., 1985. The Si:C:N ratio of marine diatoms: interspecific variability and the effect of some environmental variables. Aust. J. Psychol. 21 (3), 347–357.

Cabrera-Brufau, M., Marrasé, C., Ortega-Retuerta, E., et al., 2022. Particulate and dissolved fluorescent organic matter fractionation and composition: abiotic and ecological controls in the Southern Ocean. Sci. Total Environ. 844, 156921.

Coble, P.G., 1996. Characterization of marine and terrestrial DOM in seawater using excitation – emission matrix spectroscopy. Mar. Chem. 51, 325–346.

Combes, V., Matano, R.P., 2014. A two-way nested simulation of the oceanic circulation in the Southwestern Atlantic. J. Geophys. Res. 119, 731–756.

Combes, V., Matano, R.P., 2018. The Patagonian shelf circulation: drivers and variability. Prog. Oceanogr. 167, 24–43.

Combes, V., Matano, R.P., 2019. On the origins of the low-frequency sea surface height variability of the Patagonia shelf region. Ocean Model (Oxf). 142, 101454.

Dee, et al., 2011. The ERA-interim reanalysis: configuration and performance of the data assimilation system. Q. J. Roy. Meteor. Soc. 137, 553–597.

Druffel, E.M., Williams, P.M., Bauer, J.E., Ertel, J.R., 1992. Cycling of dissolved and particulate organic matter in the Open Ocean. J. Geophys. Res. 97, 15,639–15,659.

Druffel, E.R.M., Griffin, S., Wang, N., Garcia, N.G., McNichol, A.P., Key, R.M., Walker, B. D., 2019. Dissolved organic radiocarbon in the Central Pacific Ocean. Geophys. Res. Lett. 46, 5396–5403.

Dugdale, R.C., Minas, H.J., 1995. The role of the silicate pump in driving new production. Deep-Sea Res. I 42, 697–719.

Garzón-Cardona, J.E., Martínez, A., Barrera, F., Pfaff, F., Koch, B.P., Freije, R., Gómez, E., Lara, R., 2016. The Pacific-Atlantic connection: biogeochemical signals in the southern end of the argentine shelf. J. Mar. Syst. 163, 95–101.

Garzón-Cardona, J.E., Martínez, A.M., Pantoja, S.P., Guinder, V., Koch, B., Krock, Barrera, F., Lara, R., 2019. Linking optical and chemical signatures of dissolved organic matter in the southern argentine shelf: distribution and bioavailability. J. Mar. Syst. 195, 74–82.

Garzón-Cardona, J.E., Guinder, V.A., Alonso, C., Martínez, A.M., Pantoja-Gutiérrez, G., Kopprio, G.A., Krock, B., Lara, R.J., 2021. Chemically unidentified dissolved organic carbon: A pivotal piece for microbial activity in a productive area of the northern Patagonian shelf. Mar. Environ. Res. 167, 105286.

Giesecke, R., Martín, J., Piñones, A., Höfer, J., Garcés-Vargas, J., Flores-Melo, X., Alarcón, E., Durrieu de Madron, X., Bourrin, F., González, H.E., 2021. General hydrography of the Beagle Channel, a subantarctic interoceanic passage at the southern tip of South America. Front. Mar. Sci. 8, 621822.

Gonçalves-Araujo, R., Stedmon, C.A., Heim, B., Dubinenkov, I., Kraberg, A., Moiseev, D., Bracher, A., 2015. From fresh to marine waters: characterization and fate of dissolved organic matter in the Lena River Delta region, Siberia. Front. Mar. Sci. 2, 108.

Grasshoff, K., Ehrhardt, M., Kremling, K. (Eds.), 1999. Methods of Seawater Analysis, 3rd Received and, extended edition. Wiley-VCH, Weinheim, pp. 1–600.

Guerrero, R.A., Piola, A.R., 1997. Masas de agua en la plataforma continental, en El Mar Argentino y sus recursos pesqueros. INIDEP, Mar del Plata, Argentina, 1, pp. 107–118.

Guihou, K., Piola, A.R., Palma, E.D., Chidichimo, M.P., 2020. Dynamical connections between large marine ecosystems of austral South America based on numerical simulations. Ocean Sci. 16, 271–290.

Guinder, V.A., Malits, A., Ferronato, C., Krock, B., Garzón-Cardona, J.E., Martínez, A., 2020. Microbial plankton configuration in the epipelagic realm from the Beagle Channel to the Burdwood Bank, a marine protected area in sub-Antarctic waters. PLoS One 15 (5), e0233156.

Hammer, O., Harper, D.A.T., Ryan, P.D., 2001. PAST: paleontological statistic software package for education and data analysis. Paleontol. Eletron. 4, 1–9.

Hanckel, K., Hovland, E.K., Volent, Z., Pettersen, R., Johnsen, G., Moline, M., Sakshaug, E., 2014. Optical properties of CDOM across the polar front in the Barents Sea: origin, distribution and significance. J. Mar. Syst. 130, 219–227.

Hansen, A.M., Kraus, T.E., Pellerin, B.A., Fleck, J.A., Downing, B.D., Bergamaschi, B.A., 2016. Optical properties of dissolved organic matter (DOM): effects of biological and photolytic degradation. Limnol. Oceanogr. 61, 1015–1032.

Holm-Hansen, O., Lorenzen, C.J., Holmes, R.W., 1965. Fluorometric determination of chlorophyll. J. Conseil Intern. Pour l'Explor. Mer. 30, 3–15.

Huguet, A., Vacher, L., Relexans, S., Saubusse, S., Froidefond, J.M., Parlanti, E., 2009. Properties of fluorescent dissolved organic matter in the Gironde estuary. Org. Geochem. 40, 706–719.

Iachetti, C.M., Lovrich, G., Alder, V., 2021. Temporal variability of the physical and chemical environment, chlorophyll and diatom biomass in the euphotic zone of the Beagle Channel (Argentina): evidence of nutrient limitation. Prog. Oceanogr. 195, 102576.

Ishiwatari, R., 1992. Macromolecular material (humic substance) in the water column and sediments. Mar. Chem. 39, 151–166.

Iturraspe, R., Sottini, R., Schroeder, C., Escobar, J., 1989. Hidrología y Variables Climáticas del Territorio de Tierra del Fuego, vol. 7. Información Básica. Contribución Científica CADIC, Ushuaia, p. 201.

Kattner, G., Becker, H., 1991. Nutrients and organic nitrogenous compounds in the marginal ice zone of the Fram Strait. J. Mar. Syst. 2, 385–394.

Krock, B., Borel, C.M., Barrera, F., Tillmann, U., Fabro, E., Gaston, O., Almandoz, M.F., Garzón Cardona, J.E., Koch, B.P., Alonso, C., Lara, R., 2015. Analysis of the hydrographic conditions and cyst beds in the san Jorge gulf, Argentina, that favour dinoflagellate population development including toxigenic species and their toxins. J. Mar. Syst. 148, 86–100.

Lara, R.H., Alder, V., Franzosi, C.A., Kattner, G., 2010. Characteristics of suspended particulate organic matter in the southwestern Atlantic: influence of temperature, nutrient and phytoplankton features on the stable isotope signature. Mar. Syst. 79, 199–209.

Li, M., Xie, W., Li, P., Yin, K., Zhan, C., 2020. Establishing a terrestrial proxy based on fluorescent dissolved organic matter from sediment pore waters in the East China Sea. Water Res. 182, 116005.

Matano, R.P., Combes, V., Piola, A.R., Guerrero, R., Palma, E.D., Strub, P.T., James, C., Fenco, H., Chao, Y., Saraceno, M., 2014. The salinity signature of the cross-shelf exchanges in the southwestern Atlantic Ocean: numerical simulations. J. Geophys. Res. 119, 7949–7968.

Matano, R.P., Palma, E.D., Combes, V., 2019. The Burdwood Bank circulation. J. Geophys. Res. Oceans 124, 6904–6926.

McKnight, D.M., Boyer, E.W., Westerhoff, P.K., Doran, P.T., Kulbe, T., Andersen, D.T., 2001. Spectrofluorometric characterization of dissolved organic matter for indication of precursor organic material and aromaticity. Limnol. Oceanogr. 46, 38–48.

Møller, E., 2007. Production of dissolved organic carbon by sloppy feeding in the copepods *Acartia tonsa*, *Centropages typicus*, and *Temora longicornis*. Limnol. Oceanogr. 52 https://doi.org/10.4319/lo.2007.52.1.0079.

Murphy, K.R., Stedmon, C.A., Waite, T.D., Ruiz, G.M., 2008. Distinguishing between terrestrial and autochthonous organic matter sources in marine environments using fluorescence spectroscopy. Mar. Chem. 108 (1–2), 40–58.

Murphy, K.R., Butler, K.D., Spencer, R.G.M., Stedmon, C.A., Boehme, J.R., Aiken, G.R., 2010. Measurement of dissolved organic matter fluorescence in aquatic environments: an interlaboratory comparison. Environ. Sci. Technol. 44 (24), 9405–9412.

Palma, E.D., Matano, R.P., 2012. A numerical study of the Magellan plume. J. Geophys. Res. 117, C05041.

Palma, E.D., Matano, R.P., Piola, A.R., 2008. A numerical study of the Southwestern Atlantic shelf circulation: stratified ocean response to local and offshore forcing. J. Geophys. Res. 113, C11010.

Palma, E.D., Matano, R.P., Combes, V., 2021. Circulation and cross-shelf exchanges in the Malvinas Islands shelf region. Prog. Oceanogr. 198, 102666.

Panella, S., Michelato, A., Perdicaro, R., Magazzú, G., Decembrini, F., Scarazzato, P., 1991. A preliminary contribution to understanding the hydrological characteristics of the Strait of Magellan: austral spring 1989. Boll.i Oceanol. Teorica Appl. 9 (2–3 special issue), 107–126.

Paparazzo, F.E., Esteves, J.L., 2018. Surface macronutrient dynamics of the Drake Passage and the argentine sea. In: Hoffmayer, M.S., Sabatini, M.E., Brandini, F.P., Clliari, D.L., Santinelli, N.H. (Eds.), Plankton Ecology of the Southwestern Atlantic: From the Subtropical to the Subantarctic Realm. Springer International Publishing AG, pp. 71–86.

Paparazzo, F.E., Bianucci, L., Schloss, I.R., Almandoz, G.O., Solís, M., Esteves, J.L., 2010. Cross-frontal distribution of inorganic nutrients and chlorophyll-a on the Patagonian Continental Shelf of Argentina during summer and fall. RBMO 45, 107–119.

Paparazzo, F.E., Alder, V., Schloss, I.R., Bianchi, A., Esteves, J.L., 2016. Spatial and temporal trends in the distribution of macronutrients in surface waters of the Drake Passage. Ecol. Austral 26, 027–039.

Piola, A.R., Gordon, A.L., 1989. Intermediate waters in the southwest South Atlantic. Deep Sea res. Part I Oceanogr. Res. Pap. Deep-Sea Res Pt I. 36, 1–16.

Sabatini, M., Reta, R., Matano, R., 2004. Circulation and zooplankton biomass distributionover the southern Patagonian shelf during late summer. Cont. Shelf Res. 24, 1359–1373.

Sabatini, M.E., Reta, R., Lutz, V.A., Segura, V., 2016. Influence of oceanographic features on the spatial and seasonal patterns of mesozooplankton in the southern Patagonian shelf (Argentina, SW Atlantic). J. Mar. Syst. 157, 20–38.

Sánchez-Pérez, E.D., Pujo-Pay, M., Ortega-Retuerta, E., Conan, P., Peters, F., Marrasé, C., 2020. Mismatched dynamics of dissolved organic carbon and chromophoric dissolved organic matter in the coastal NW Mediterranean Sea. Sci. Total Environ. 746, 141190.

Senesi, N., Miano, N.T., Provenzano, M.R., Brunetti, G., 1991. Characterization, differentiation and classification of humic substances by fluorescence spectroscopy. Soil Sci. 152, 259–271.

Sigman, D.M., Altabet, M.A., McCorkle, D.C., Francois, R., Fischer, G., 2000. The $\delta^{15}N$ of nitrate in the Southern Ocean: nitrogen cycling and circulation in the ocean interior. J. Geophys. Res. 105 (C8), 19599–19614.

Skoog, A., Thomas, D., Lara, R., Richter, K., 1997. Methodological investigations on DOC determinations by HTCO method. Mar. Chem. 56, 39–44.
Stedmon, C.A., Bro, R., 2008. Characterizing dissolved organic matter fluorescence with parallel factor analysis: a tutorial. Limnol. Oceanogr. Methods 6, 572–579.
Strub, P.T., James, C., Combes, V., Matano, R.P., Piola, A.R., Palma, E.D., Saraceno, M., Guerrero, R.A., Fenco, H., Ruiz-Etcheverry, L.A., 2015. Altimeter-derived seasonal circulation on the southwest a tlantic shelf: 27°-43° S. J. Geophys. Res. 120, 3391–3418.
Yamashita, Y., Hashihama, F., Saito, H., Fukuda, H., Ogawa, H., 2017. Factors controlling the geographical distribution of fluorescent dissolved organic matter in the surface waters of the Pacific Ocean. Limnol. Oceanogr. 62 (2017), 2360–2374.
Zakem, E.J., Al-Haj, A., Church, M.J., van Dijken, G.L., Dutkiewicz, S., Foster, S.Q., Fulweiler, R.W., Mills, M.M., Follows, M.J., 2018. Ecological control of nitrite in the upper ocean. Nat. Commun. 9, 1206.
Zhou, Y., Martin, P., Müller, M., 2019. Composition and cycling of dissolved organic matter from tropical peatlands of coastal Sarawak, Borneo, revealed by fluorescence spectroscopy and parallel factor analysis. Biogeosciences 16, 2733–2749.
Zsolnay, A., Baigar, E., Jimenez, M., Steinweg, B., Saccomandi, F., 1999. Differentiating with fluorescence spectroscopy the sources of dissolved organic matter in soils subjected to drying. Chemosphere 38, 45–50.